Moroccan Journal of Chemistry
ISSN : 2351-812X

Mor. J. Chem., 2023, Volume 11, Issue 4, Page 1266-1286
https://revues.imist.ma/index.php/morjchem
https://doi.org/10.48317/IMIST.PRSM/morjchem-v11i04.42045

Molecular Docking against SARS-CoV-2 Variants, Antiviral Effects, Dynamics and Quantum Chemical Modeling of Mannopyranoside Derivatives

Sarkar M. A. Kawsar[a*], Jannatul Ferdous[a], Mohammed K. Hossain[b], Ajoy Kumer[c], Shopnil Akash[d], Unesco Chakma[e]

[a] *Lab of Carbohydrate and Nucleoside Chemistry (LCNC), Department of Chemistry, Faculty of Science, University of Chittagong, Chittagong-4331, Bangladesh*
[b] *Department of Pharmacy, Faculty of Biological Science, University of Chittagong, Chittagong-4331, Bangladesh*
[c] *Laboratory of Computational Research for Drug Design and Material Science, Department of Chemistry, European University of Bangladesh, Dhaka 1216, Bangladesh*
[d] *Department of Pharmacy, Faculty of Allied Health Sciences, Daffodil International, University, Dhaka, Bangladesh*
[e] *Department of Electrical and Electronics Engineering, European University of Bangladesh, Gabtoli, Dhaka-1216, Bangladesh*
**Corresponding author, Email address: akawsarabe@yahoo.com*

Received *05 Aug 2023,*
Revised *23 Sept 2023,*
Accepted *24 Sept 2023*

Citation*: Kawsar S. M. A., Ferdous J., Hossain M. K., Kumer A., Akash S., Chakma U. (2023) Molecular Docking against SARS-CoV-2 Variants, Antiviral Effects, Dynamics and Quantum Chemical Modeling of Mannopyranoside Derivatives, Mor. J. Chem., 11(4), 1266-1286*

Abstract: The emergence of the SARS-CoV-2 virus in the latter part of 2019 initiated a worldwide pandemic, exerting major impacts on both public health and the global economy. Researchers from across the globe have been actively engaged in conducting thorough investigations on possible therapeutic interventions and vaccines aimed at mitigating the impact of the virus. This work aimed to comprehensively investigate the antiviral efficacy of several methyl α-D-mannopyranoside compounds and their derivatives against six distinct strains of SARS-CoV-2, including the alpha, beta, gamma, delta, and omicron variants. The present study was undertaken to investigate the computational properties of methyl α-D-mannopyranoside and its designed derivatives to assess their thermophysical and biochemical parameters. The PASS prediction score was reported to be 0.233<Pa<0.403 for antiviral, 0.473<Pa<0.569 for antibacterial, 0.628<Pa<0.680 for antifungal, and 0.242<Pa<0.349 for antibiotic. For this purpose, previously synthesized potential derivatives of methyl α-D-mannopyranoside were assessed with six different variants of the COVID-19 protein and docking studies by AutoDock. Molecular docking experiments were performed in order to assess the binding affinity between α-D-mannopyranoside derivatives and the spike glycoprotein of SARS-CoV-2, as well as its variations. The ligand L06 exhibited superior binding affinity compared to the FDA-approved Molnupiravir, across all variations. The stability of the docked complexes was validated using molecular dynamics simulations, indicating that L06 has the potential to be an efficacious therapy for different types of SARS-CoV-2. The substances under investigation had favorable pharmacokinetic features as determined by ADMET (absorption, distribution, metabolism, excretion, and toxicity) study. Therefore, this methyl-α-D-mannopyranoside and its derivatives might be useful to inhibit the mentioned COVID-19 variants as a potential drug(s) candidate.

Keywords: Spike glycoprotein alpha, beta and delta variant; Docking; Molecular dynamics; PASS; ADMET

1. Introduction

The epidemic of respiratory disease was diagnosed in a cluster of pneumonia patients in Wuhan, China, in December 2019 (Shuxian *et al.*, 2020). Within a few days, the virus spread throughout the city of Wuhan, infecting a large number of people and killing many more (Touzani *et al.*, 2020; Bendaif *et al.*, 2020). As time goes on, the spread of the virus increases, and in a very short period, the virus spreads all over the world, and many people have died except on the continent of Antarctica (Hosen *et al.*, 2022). The World Health Organization (WHO) issued a red alert as an epidemic on March 11, 2020 (Islam *et al.*, 2022). This has resulted in the collapse of the world economy (Zhang *et al.*, 2020; Cucinotta *et al.*, 2020) and is considered a significant health concern from a global perspective (Amin *et al.*, 2021a). Since then, scientists in different countries have identified various features of this tiny pathogenic virus. For example, the transmembrane spike glycoproteins of this coronavirus are responsible for allowing it to penetrate the human host (Amin *et al.*, 2021b), and the size of this virus is approximately 50-200 nanometers (Huang *et al.*, 2020). It is an RNA virus that has four different proteins: S (spike), E (envelope), M (main protease) and N (nucleocapsid) (Paraskevis *et al.*, 2020). In addition, the first variant of the virus was detected in Wuhan Province (Tang *et al.*, 2020), and the virus has become increasingly pathogenic by a mutant of its genomic character and spread very quickly (Zucman *et al.*, 2021). Among them, some of the notable variants that affect most people and kill most people are the alpha variant (Xia *et al.*, 2021), beta variant, gamma variant, delta variant (Li *et al.*, 2021) and Omicron variant (Karim *et al.*, 2021), and some studies have shown that the new delta variant is 70-80% more aggressive than the other coronavirus strains (Adrian *et al.*, 2021).

Scientists are now trying to investigate and develop an effective therapeutic target to fight against this infection by identifying a particular medicine or vaccine that may block viral replication as soon as feasible (Arifuzzaman *et al.*, 2018; Farhana *et al.*, 2021; Kabir *et al.*, 2009a). Simultaneously, computational technologies such as molecular docking and molecular dynamics (MD), pharmacokinetic profiling and Lipinski rule parameters, and absorption, distribution, metabolism, excretion and toxicity (ADMET) have gained prominence as key prospects for investigating possible inhibitors against SARS-CoV-2 (Aanouz *et al.*, 2021; Saputra *et al.*, 2022; Diass *et al.*, 2023).

Carbohydrates are a kind of natural substance that refers to the bioorganic chemical class present in all biological species on the planet, and they are engaged in a variety of biological activities (Kawsar *et al.*, 2009), including glycolysis and glycogenesis (Kawsar *et al.*, 2021a, 2015; Misbah *et al.*, 2020; Shagir *et al.*, 2016), along with providing energy. They also play a significant role in a variety of biochemical signaling pathways and recognize activities such as the immunological response to inflammation (Weymouth-Wilson *et al.*, 1997; Fujii *et al.*, 2011; Kabir *et al.*, 2004, 2008).

Methyl α-D-mannopyranoside is one of the most significant and potent classes of carbohydrates due to the numerous biological applications of its derivatives. Methyl α-D-mannopyranoside and its derivatives have demonstrated multiple bioactivities, such as antibacterial, antifungal, antitumor, antiviral, antidiabetic, and anti-inflammatory activities (Kawsar *et al.*, 2011, 2014; Alam *et al.*, 2021; Bulbul *et al.* 2021a). Hence, a series of methyl α-D-mannopyranosides and their derivatives was developed to explore its antiviral activity using biological prediction, molecular docking engagement, pharmacokinetic and toxicity analysis. These derivatives were then subjected to a molecular docking simulation to determine the binding affinity and nonbonding interaction of the receptor protein of six different variants of the SARS-CoV-2 virus, spike glycoprotein, alpha, beta, gamma, delta, and Omicron variants. Then, molecular dynamics simulations were carried out for 100 ns to validate the

stability of the docked complexes. Moreover, pharmacokinetic modeling has been used to investigate the absorption, metabolism, and toxicity of the substances.

2. Methodology

2.1 Ligand optimization and DFT calculation frequency

Six chemically synthesized methyl α-D-mannopyranoside compounds were developed, and geometry optimization was accomplished with the application of Material Studio 8.0 (Kumar *et al.*, 2021). The B3LYP of the DMol3 code program was utilized to optimize the ligands and compute the chemical reactivity markers by the DFT program. DFT frequency calculations were implemented to evaluate the chemical reactivity parameters (Becke *et al.*, 1988; Parr *et al.*, 1980). Then, the molecular frontier orbital schematic of the highest occupied molecular orbital (HOMO) and lowest unoccupied molecular orbital (LUMO) was redrawn using analytical techniques, and the electrostatic potential map was generated. Finally, the optimized structure was exported in PDB format and uploaded in PyRx AutoDock Vina for molecular docking against the targeted protein.

2.2 PASS prediction

The online machine learning web tool PASS (http://www.pharmaexpert.ru/passonline/) was implemented to measure the antibacterial, antiviral, antifungal, and antineoplastic activity spectra of reported derivatives of the mentioned compounds (Kawsar *et al.*, 2021b). Antibacterial, antiviral, antifungal, and antineoplastic activity spectra could be generated using the PASS server by drawing substances and then converting them to SMILES format using SwissADME online tools. There are two types of PASS results: the probability of active molecules (Pa) and the probability of inactive molecules (Pi). From 0.00 to 1.00, the Pa and Pi scores are generally not equal to one (Pa + Pi ≠1). Pass prediction has been applied to select a suitable drug target.

2.3 Pharmacokinetics and drug-likeness investigation

Lipinski's rule is used to measure the drug-likeness characteristics of small molecular compounds (Lipinski *et al.*, 2001). Due to many unwanted reasons, a large number of prospective therapeutic candidates could not reach the final stages. Therefore, before conducting a laboratory experiment, Lipinski's rule was used to determine the likely pharmacokinetic characteristics of a possible medication candidate. Numerous potential candidates could not be capable of becoming successful for a multitude of reasons. Therefore, Lipinski's rule was used to identify the probable pharmacokinetic features of a potential drug candidate before going to a laboratory experiment. The online web tool SwisADME (http://www.swissadme.ch/index.php) was used (Daina *et al.*, 2017) and takes required pharmacokinetic data, including topological polar surface area, the logarithm of partition coefficient between n-octanol and water, number of rotatable bonds, hydrogen bond acceptor, hydrogen bond donor, molecular weight, gastrointestinal absorption, etc.

2.4 Protein preparation and molecular mocking study and visualization

The initial three-dimensional (3D) configuration of SARS-CoV-2, six different variant proteins such as SARS-CoV-2 spike glycoprotein, alpha, beta, gamma, delta, and omicron variant, was acquired from the Protein Data Bank (PDB), which has been found at the URL following "https://www.rcsb.org/structure/". All three-dimensional protein structures were viewed using PyMOL, V2.3, a version of the PyMOL modeling program (https://pymol.org/2/) (Delano *et*

al., 2002). To generate a clean structure of the proteins, all water molecules and unwanted compounds or substituents were eliminated by PyMOL application, and their energy was minimized with the help of Swisspdbviwer and saved in PDB format. PyRx software was implemented for molecular docking as part of AutoDock Vina. In view of molecular docking, the fresh three-dimensional protein and optimized structures were uploaded in the PyRx application and converted into macromolecules. Finally, molecular docking was performed, and the binding energy was calculated. Notably, the spike protein of SARS-CoV-2 variants was used in this current investigation (El Aissouq *et al.*, 2023; Khatabi *et al*., 2022). The main reason for selecting the spike protein is that the spike protein plays an essential role in viral infection and pathogenicity. The host receptor is recognized and bound by the spike protein, and then conformations in the spike protein allow the viral envelope to fuse with the host cell membrane. Following the molecular docking procedure, the docked complex was imported into Discovery Studio version 2021 for further analysis and visualization (A. S Inc.). The grid center points were set to wrap the protein substrate-binding site, and the grid box measurements are displayed in Table 1. The targeted protein information is also listed in Table 2.

Table 1. Grid box parameters used for docking analysis in this study for different SARS-CoV-2 variants

Protein name	**Grid box size**	
	Center	**Dimension (Å)**
SARS-CoV-2 spike glycoprotein	X = 210	X = 119
	Y = 210	Y = 125
	Z = 207	Z = 158
SARS-CoV-2 Alpha variant	X = 27	X = 62
	Y = 18	Y = 71
	Z = 14	Z = 111
SARS-CoV-2 Beta variant	X = 27	X = 63
	Y = 18	Y = 70
	Z = 14	Z =111
SARS-CoV-2 Gamma variant	X = 212	X=89
	Y = 196	Y =61
	Z = 171	Z=112
SARS-CoV-2 Delta variant	X = 210	X = 131
	Y = 211	Y = 131
	Z = 215	Z = 185
SARS-CoV-2 Omicron variant	X = 200	X = 64
	Y = 160	Y = 73
	Z = 266	Z = 108

Table 2. Three-dimensional protein structure of the targeted protein (different SARS-CoV-2 variants)

Title	SARS-CoV-2 spike glycoprotein (PDB ID: 6vxx)	SARS-CoV-2 Alpha variant (PDB ID: 7EKF)	*SARS-CoV-2 Beta variant (*PDB ID: *7ekg)*
Organism	Severe acute respiratory syndrome coronavirus	*Homo sapiens*	*Homo sapiens*
Resolution	2.80 Å	2.85 Å	2.63 Å

3D structure of protein	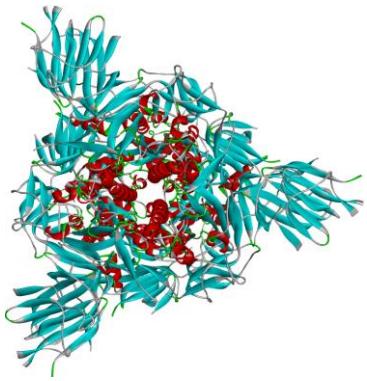	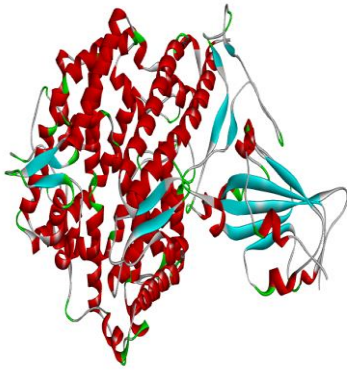	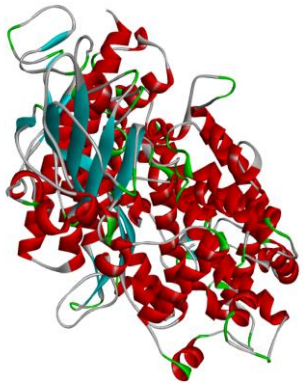
References	(Alam *et al.*, 2022)	(Maowa *et al.*, 2021a)	(Maowa *et al.*, 2021b)
Title	*SARS-CoV-2* Gamma variant (PDB ID: 7V84)	*SARS-CoV-2 Delta variant* (PDB ID: 7*V8B)*	*SARS-CoV-2* Omicron variant (PDB ID: 7T9J)
Organism	Severe acute respiratory syndrome coronavirus	Severe acute respiratory syndrome coronavirus	Severe acute respiratory syndrome coronavirus
Resolution	3.00 Å	3.20 Å	2.79 Å
3D structure of protein	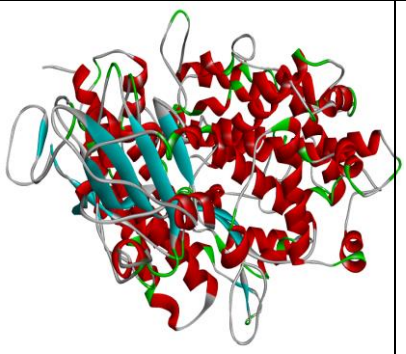	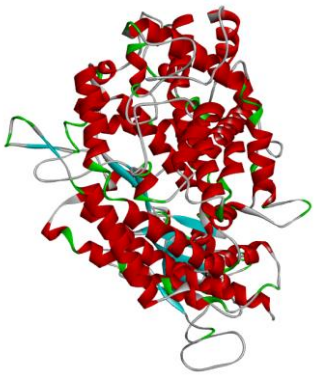	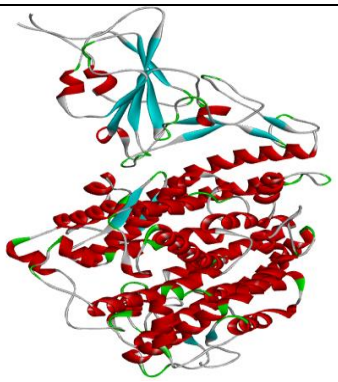
References	(Bulbul *et al.*, 2021b)	(Mandal *et al.*, 2022)	(Alam *et al.*, 2021)

2.6 Molecular dynamics

NAMD software was used to execute interactive molecular dynamics of the best three docking scores on a high-configuration laptop computer (Phillips *et al.*, 2005). To analyze the docking findings obtained for the top ligand-SARS-CoV-2 binding proteins. MD simulations were performed up to 100 ns using the AMBER14 force field (Case *et al.*, 2005). The whole unit was evenly balanced with 0.9% NaCl at 298 K in the presence of a liquid medium. To simulate the procedure and the boundary conditions, a cubic cell was cycled within a 20 Å range on either side of the process and the boundaries. Then, the root-mean-square deviation (RMSD) and root mean square fluctuation (RMSF) were calculated using the VMD program once the simulations had been completed (Chtita *et al.*, 2022; Soudani *et al.*, 2023).

2.7 ADMET prediction

Biological absorption, distribution, metabolism, excretion, and toxicity (ADMET) plays significant roles in new bioactive molecule discovery and development (Guan *et al.*, 2019). Many drugs cannot reach the commercial stage due to the failure of suitable ADMET features. Therefore, in this study, the ADMET features were investigated by implementing the online databases pkCSM (http://biosig.unimelb.edu.au/pkcsm/prediction_single/adme_1643643729.19) and SwissADME (Kumar *et al.*, 2021). Water solubility Log S, Caco-2 permeability, P-glycoprotein substrate, P-I

glycoprotein inhibitor VDss (human), BBB permeability, CYP450 1A2, inhibitor CYP450 2C9 substrate, total clearance, renal OCT2 substrate, maximum tolerated dose, etc., are the primary concerns.

3. Results and Discussion

Some well-known carbohydrates with a glucose group, including methyl-α-D-mannopyranoside (Figure 1), are efficient against a broad spectrum of microorganisms. Consequently, this investigation was recognized, and computer modeling was carried out against different variants of SARS-CoV-2. This study's main objective is to identify a potent medication against SARS-CoV-2's different variants.

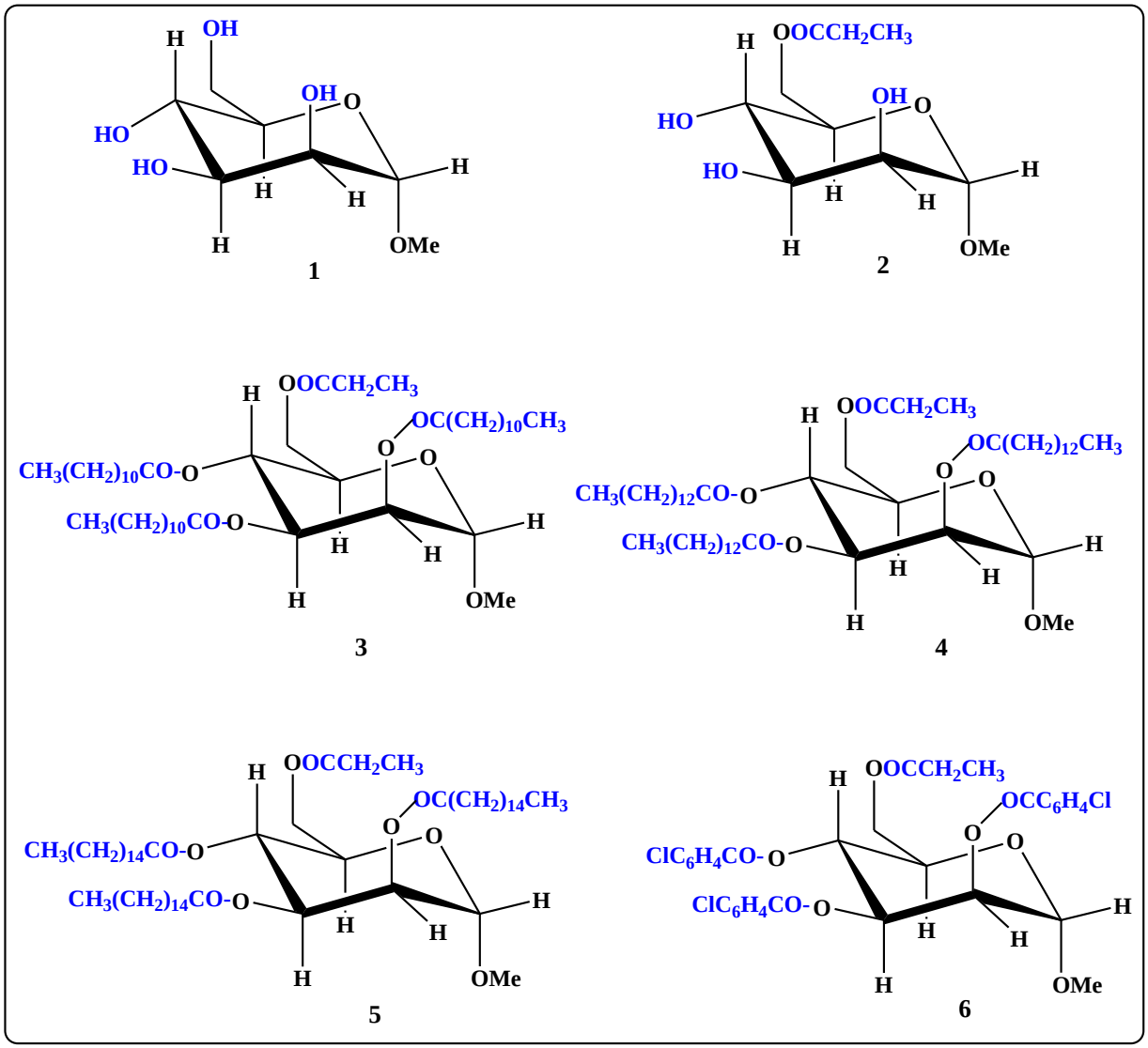

Figure 1. Chemical structure of methyl α-D-mannopyranoside derivatives

3.1 Optimized structure of the tested ligand

DFT functions were implemented for the equilibrium and ligand geometry optimization of the six methyl-α-D-mannopyranosides and their modified structures at B3LYP/6-31G. The optimized chemical structures of these derivatives are highlighted in Figure 2, which depicts the completely optimized compound that was considered to be the most consistent and stable.

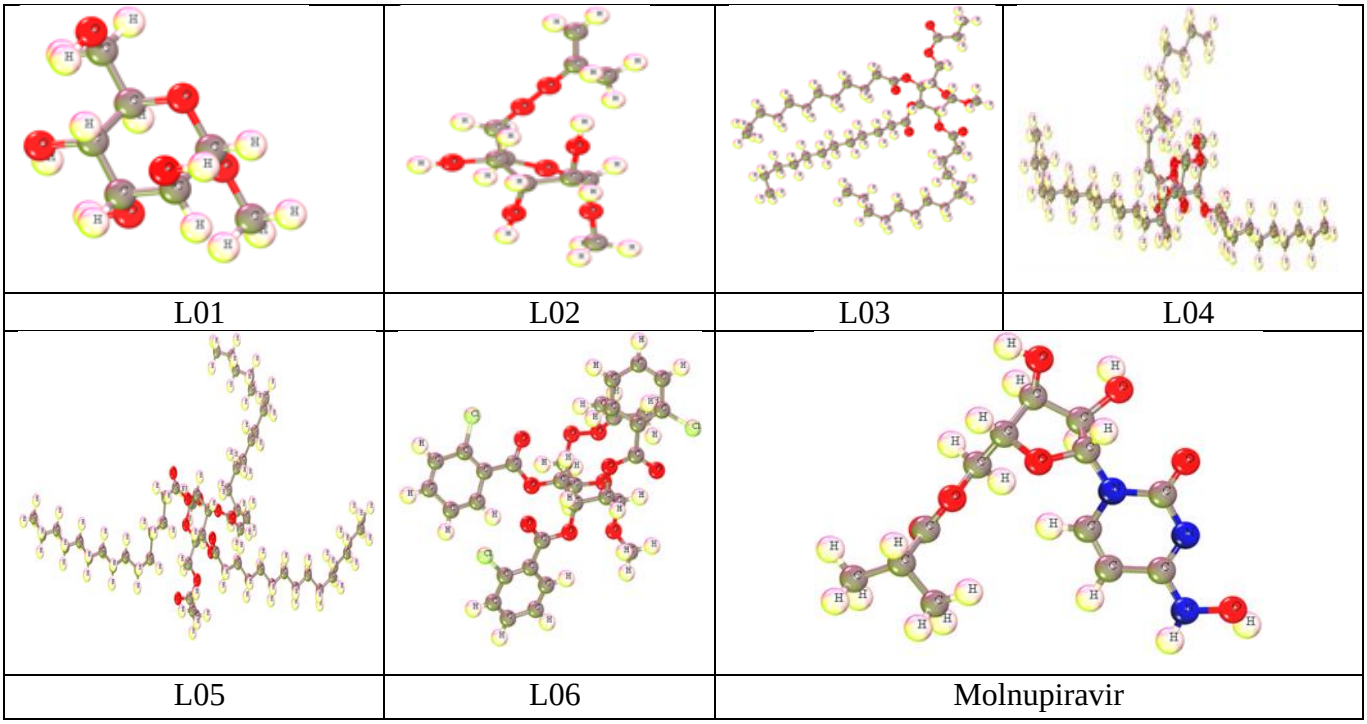

Figure 2. Optimized structures

3.1 Pharmacokinetics and drug-likeness investigation

Therapeutic likeness is a qualitative evaluation of the biochemical responsiveness of a certain small molecular molecule or scientifically developed prospective drug target. Improved efficiency and efficacy in the conception of novel drugs are dependent on the development of reliable computer models for the detection of prospective substances in computational chemistry. From the viewpoint of the Lipinski rule, only ligands L01 and L02 can maintain the five rules, and the other molecules cannot fulfill them due to extensive molecular weight (Table 3).

Table 3. Data on the Lipinski rule, pharmacokinetics and drug-likeness

Entry	NBR	HBA	HBD	TPSA, Å²	Consensus Log Po/w	Log Kp (skin permeation), cm/s	Lipinski rule		M.W.	Bioavailability Score	G.I. absorption
							Result	Violation			
L01	02	06	04	99.38	-1.64	-9.37	Yes	00	194.18	0.55	Low
L02	05	07	03	97.61	-0.47	-8.47	Yes	00	250.25	0.55	High
L03	42	10	00	107.98	11.28	0.71	No	02	799.17	0.17	Low
L04	46	10	00	123.66	13.00	1.44	No	02	867.29	0.17	Low
L05	52	10	00	123.66	15.00	3.23	No	02	951.45	0.17	Low
L06	14	10	00	115.82	5.60	-4.91	No	02	665.90	0.17	Low
Molnupiravir	06	08	04	143.14	-1.16	-9.26	Yes	00	329.31	0.55	Low

[Abbreviations: TPSA: topological polar surface area, consensus log: logarithm of partition coefficient between n-octanol and water**,** NBR: number of rotatable bonds**,** HBA: hydrogen bond acceptor, HBD: hydrogen bond donor**,** M.: molecular weight, G.I. Absorption: gastrointestinal absorption].

Therefore, the molecular weight has been denied, and further studies have been carried out. Second, almost all the drugs have a minimum GI absorption rate, with only ligands L01 and L02 having higher oral bioavailability, which indicated that all of these drugs could take a long time to absorb in the gastrointestinal tract.

3.2 PASS prediction

Pa and Pi have been used to represent the PASS findings, which are noted in Table 4. The predicted Pa scores were 0.233 < 0.408 for antiviral, 0.473< 0.569 for antibacterial, 0.632 < 0.680 for antifungal and 0.242 < 0.349 for antibiotic (Table 4). The PASS outcomes indicate that the Pa value is very low for antiviral targets compared to antibacterial, antifungal and antibiotic targets. However, the experimental data that have been previously obtained in the laboratory described that these molecules could be effective against viral pathogens. Therefore, although the Pa score is lower for antiviral therapy, this study has been continued for further investigation based on experimental values.

Table 4. Data of pass prediction

Entry	Antiviral		Antibacterial		Antifungal		Antibiotic	
	Pa	Pi	Pa	Pi	Pa	Pi	Pa	Pi
L01	0.403	0.014	0.541	0.013	0.628	0.016	0.349	0.010
L02	0.366	0.020	0.542	0.013	0.649	0.013	0.343	0.011
L03	0.233	0.071	0.473	0.019	0.632	0.015	0.271	0.017
L04	0.293	0.039	0.569	0.011	0.680	0.011	0.344	0.010
L05	0.293	0.039	0.569	0.011	0.680	0.011	0.344	0.010
L06	0.308	0.034	0.475	0.019	0.648	0.014	0.242	0.021
Molnupiravir	0.599	0.05	0.241	0.088	0.257	0.102	0.134	0.057

3.2 Molecular orbitals and chemical reactivity descriptor

Table 5 shows the computationally calculated highest occupied molecular orbital (HOMO), lowest unoccupied molecular orbital (LUMO), E gap, chemical potential, electronegativity, hardness, softness (s) and electrophilicity of methyl α-D-mannopyranoside. The B3LYP operation was used to generate the values of the reported molecule. According to the LUMO, the HOMO energy gap and chemical permeability may be assessed. Substantial LUMO and HOMO gaps indicate high mobility and poor chemical stability (Kawsar *et al.*, 2021c; Kawasr *et al.*, 2020a). The range of the energy gap was reported at 6<9 eV for all investigated medicines, with ligand L02 showing the lowest HOMO–LUMO distance and the greatest softness value (-0.3039). The maximum hardness is approximately 4 in ligand L05, where the best softness was reported for ligand L02 (-0.2099). The chemical descriptor data indicate that they should be used as potent and bioactive molecules for future use (El Hadki *et al.*, 2021).

3.2 Frontier molecular orbitals (FMOs)

The frontier molecular orbitals of HOMO and LUMO are symbolized in Figure 3 by various colors for clear understanding, which are assumed to differentiate between chemical reactivity and kinetic stability (Kawsar *et al.* 2020b). The smaller energy gap aids in the formation of an

engagement between medicines and the SARS-2 protein. Positive nodes are represented by the greenish color in the HOMO, whereas negative nodes are represented by the deep violet hue. Thus, the HOMO is the portion of bioactive metabolites in which the electrophilic attracting group may be joined to produce the chemical interaction, and the LUMO is the positive domain of the structure in which the nucleophilic group can be introduced. The negative part of the orbital is represented by lime green, while the positive part is represented by deep radish. Generally, it is stated that the protein may be coupled to the LUMO portion of the molecule. The FMO values for the mentioned molecules are differentiated by different colors and displayed in Figure 3.

Table 5. Data of chemical descriptors

Entry	A=-LUMO	I=- HOMO	Energy =I-A	Chemical potential $(\mu) = -\frac{I+A}{2}$	Electronegativity $(\chi) = \frac{I+A}{2}$	Hardness $(\eta) = \frac{I-A}{2}$	Softness $(\sigma) = \frac{1}{\eta}$	Electrophilicity $(\omega) = \frac{\mu^2}{2\eta}$
L01	-2.15	-10.18	8.03	6.16	-6.16	-4.01	-0.24	-4.73
L02	-2.13	-8.58	6.45	5.35	-5.35	-3.22	-0.30	-4.44
L03	-0.59	-10.12	9.52	5.35	-5.35	-4.76	-0.20	-3.01
L04	-0.83	-10.24	9.40	5.54	-5.54	-4.70	-0.21	-3.26
L05	-0.59	-10.53	9.93	5.56	-5.56	-4.96	-0.20	-3.11
L06	-0.71	-9.17	8.46	4.94	-4.94	-4.23	-0.23	-2.88
Molnupiravir	-0.29	-9.37	9.08	4.83	-4.83	-4.54	-0.22	-2.57

3.2 Virtual screening, molecular docking, and noncovalent interactions

Molecular docking findings are generally reported in terms of how well drugs can attach to receptors as well as how many hydrogen bonds, hydrophobic bonds, and polar and nonpolar bonds are formed between them when they are docked. For the most part, the partial charge is used to form "polar bonding." between molecules and proteins. Table 6 shows the multiple numbers of hydrogen and hydrophobic bonds as well as the frameworks of amino acids with polar bonds. The standard drug-protein affinities have been regarded as -6.00 kcal/mol for potential drug molecules (Nath *et al.*, 2021; Shamsuddin *et al*., 2021; Mirajul *et al*., 2019). In this study, six distinct SARS-CoV-2 variants were selected, and docking simulations were performed. The binding affinities ranged from -4.4 kcal/mol to 8.5 kcal/mol for the substances tested. Table 6 presents the docking score with bond types against the SARS-CoV-2 spike glycoprotein, alpha variant (PDB ID: 7EKF) and beta variant (PDB ID: 7ekg). The largest binding energy was found at -8.0 kcal/mol in L06 against the SARS-CoV-2 spike glycoprotein at the same time. The SARS-CoV-2 alpha variant consists of -8.5 kcal/mol in L06, and the beta variant (PDB ID: 7ekg) of SARS-CoV-2 has been highlighted as -7.5 kcal/mol in ligand 06. The ligand 06 has been opposed to the FDA-approved Molnupiravir in spike glycoprotein, Alpha variant (PDB ID: 7EKF) and Beta variant (PDB ID: 7ekg). In addition, it is stated that the other ligands have lower binding energy compared to standard Molnupiravir.

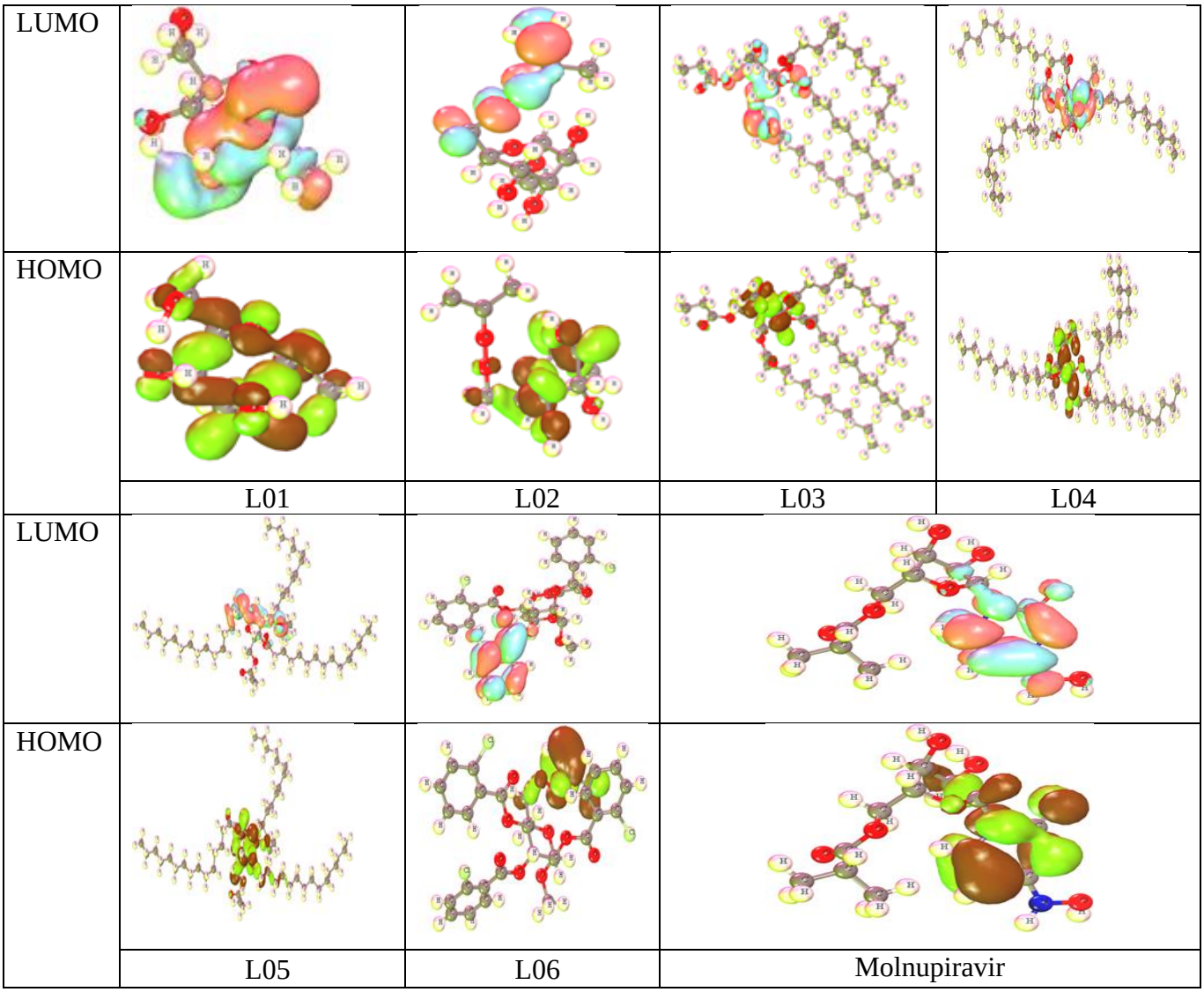

Figure 3. HOMO and LUMO diagram

Table 6. Docking score with bond types

SARS-CoV-2 Spike glycoprotein (PDB ID: 6vxx)				SARS-CoV-2 Alpha variant (PDB ID: 7EKF)			SARS-CoV-2 Beta variant (PDB ID: 7ekg)		
Entry	Binding Affinity (kcal/mol)	No of H bond	No of Hydrophobic bond	Binding Affinity (kcal/mol)	No of H bond	No of Hydrophobic bond	Binding Affinity (kcal/mol)	No of H bond	No of Hydrophobic bond
L01	-5.6	5	0	-5.3	4	0	-4.8	2	0
L02	-6.1	4	1	-5.6	2	4	-5.3	5	0
L03	-6.2	7	7	-4.6	7	5	-5.8	2	11
L04	-5.8	4	8	-6.0	4	11	-5.3	2	11
L05	-6.3	4	12	-4.4	8	8	-5.3	13	5
L06	-8.0	4	8	-8.5	0	5	-7.5	3	6
Molnupiravir	-7.9	5	2	-6.6	2	5	-7.3	5	6

In this paper, the SARS-CoV-2 spike glycoprotein, alpha variant (PDB ID: 7EKF) and beta variant (PDB ID: 7ekg) were first studied. The efficacy of the reported drug has been found to have potential against spike glycoprotein, alpha variant (PDB ID: 7EKF) and beta variant (PDB ID: 7ekg). Then, three more SARS-CoV-2 variants were selected for further investigation. After that, it has been seen that in all cases, L06 is more active and forms the highest range of binding energy (Table 7). In all cases, ligand L06 has been opposed to the standard FDA-approved drug affinities. Therefore, this potential medication will be effective for targeting the abovementioned SARS-CoV-2 variants.

Table 7. Docking score with bond types

	SARS-CoV-2 Gamma variant (PDB ID: 7V84)			SARS-CoV-2 Delta variant (PDB ID: 7V8B)			SARS-CoV-2 Omicron variant (PDB ID: 7T9J)		
Entry	**Binding Affinity (kcal/mol)**	**No of H bond**	**No of Hydrophobic bond**	**Binding Affinity (kcal/mol)**	**No of H bond**	**No of Hydrophobic bond**	**Binding Affinity (kcal/mol)**	**No of H bond**	**No of Hydrophobic bond**
L01	-5.6	3	0	-4.8	3	0	-5.0	4	0
L02	-5.5	3	1	-5.3	4	2	-5.4	6	1
L03	-4.9	7	9	-5.8	4	13	-5.3	4	7
L04	-4.6	8	4	-5.3	7	7	-5.0	10	3
L05	-4.5	4	14	-5.3	5	7	-5.2	10	6
L06	-7.3	3	6	-7.5	9	8	-7.6	4	7
Molnupiravir	-6.5	8	1	-6.9	6	5	-7.3	4	3

3.2 Molecular docking poses of SARS-CoV-2 with different variants

Active amino acid residues, molecular docking poses and hydrogen bond donors/acceptors are illustrated graphically in Figure 4. This illustration was designed with the help of PyMOL and Biovia Discovery Studio 2021. The molecular docking pose provided information on how the reported ligand bonded to the targeted protein or how engaged the drug-protein was with each.

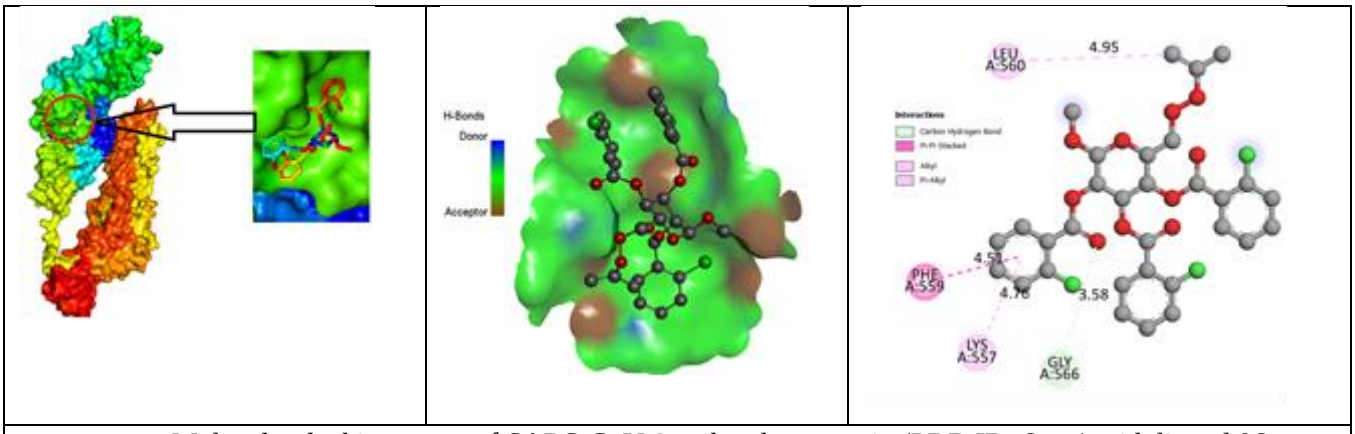

Molecular docking poses of SARS-CoV-2 spike glycoprotein (PDB ID: 6vxx) with ligand 06

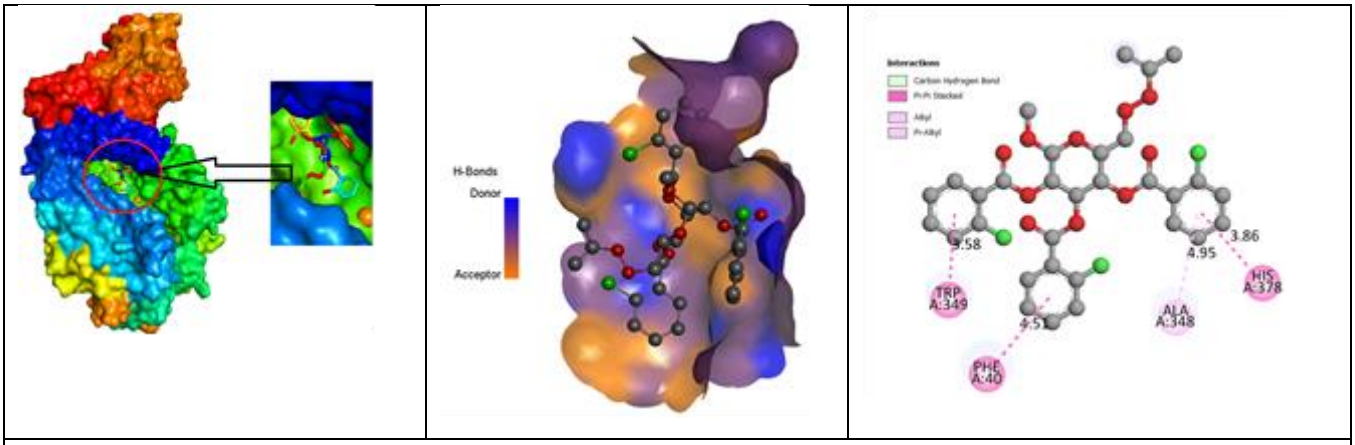

Molecular docking poses of SARS-CoV-2 Alpha variant (PDB ID: 7EKF) with ligand 06

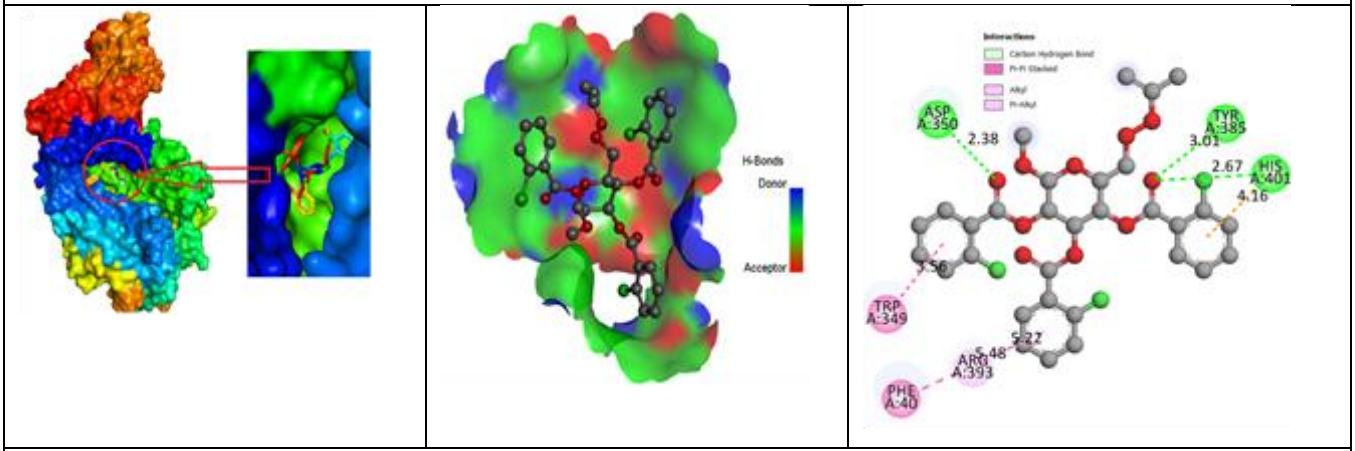

Molecular docking poses of SARS-CoV-2 Beta variant (PDB ID: 7ekg) with ligand 06

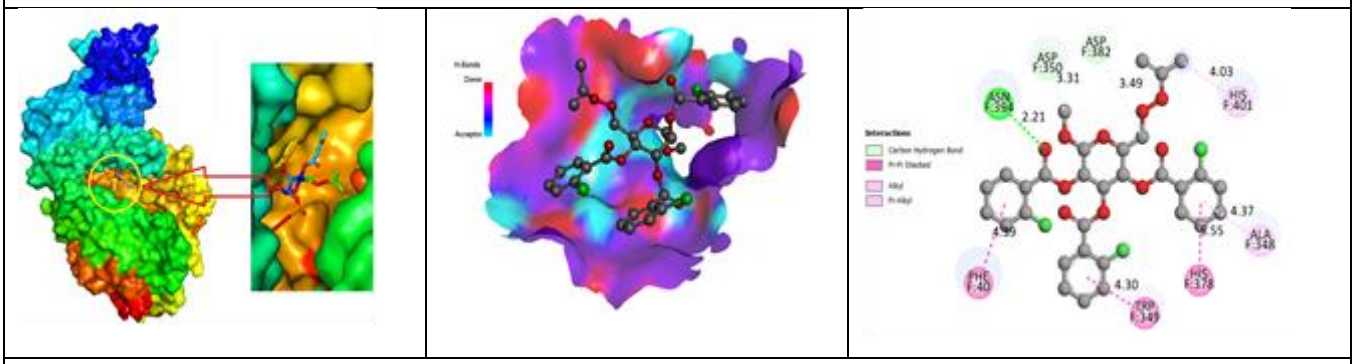

Molecular docking poses of SARS-CoV-2 Gamma variant (PDB ID: 7V84) with ligand 06

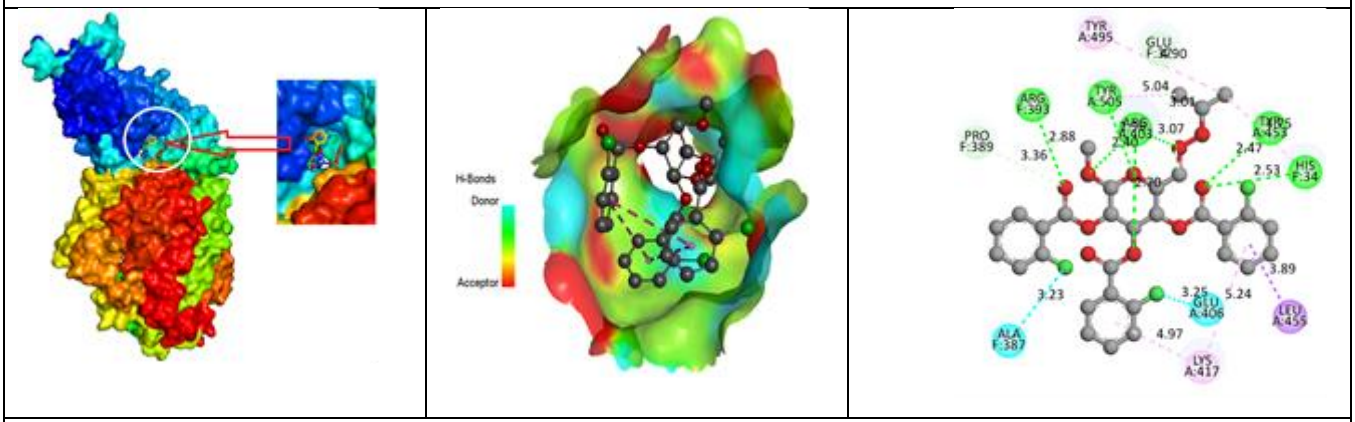

Molecular docking poses of SARS-CoV-2 Delta variant (PDB ID: 7V8B) with ligand 06

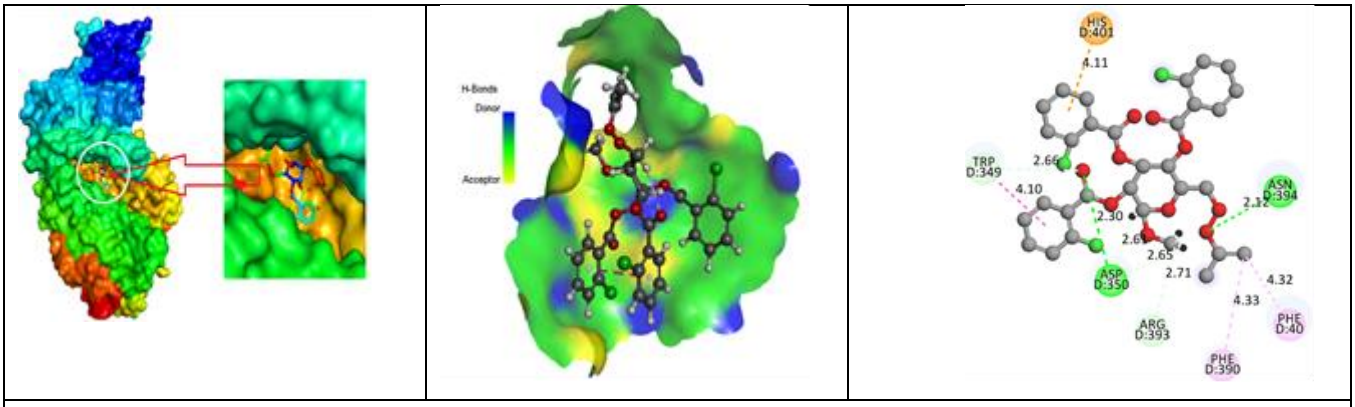

Molecular docking poses of SARS-CoV-2 Omicron variant (PDB ID: 7T9J) with ligand 06

Figure 4. Molecular docking pose and 2D structures of protein–ligand interactions

3.2 Molecular dynamics simulation

The atomic and molecular movements of a protein–ligand docked complex have been evaluated using molecular dynamics computations. The root-mean-square deviation (RMSD) is a known equation of mechanical displacement that is abbreviated as RMSD. In other words, the RMSD is described across different pairs of molecular atoms, which reveals how the protein configuration has altered between the two points. Root mean square fluctuation (RMSF), on the other hand, is an abbreviation for root mean square fluctuation, and it is a representation of how much a residual shift (fluctuates) occurs during the period of molecular dynamics simulation. These are all included in molecular dynamics, which ensure stability and docking authentication by the two terms RMSD and RMSF (Kawsar *et al*., 2022; Version ADS, 2017). The RMSD and the RMSF of ligand L06 with the reported protein were employed to determine the stabilization of docked compounds of the binding protein, small molecule engagement, and hydrogen bonding. In this work, the RMSD and the coupling of protein amino acid residues were determined at 0-100 ns. The RMSD becomes less than 2.0, as shown in Figures 5-10 (without bonds or interactions), suggesting that they perfectly match the different SARS-CoV-2 variant protein structures.

However, the RMSD shifts with the development of a backbone of amino acid residue or the development of a hydrogen bond, increasing very little following the construction of these structures. Hydrogen bonds have minimal influence on molecular docking affinity and stability and their RMSD. Hydrophobic bonds in protein–ligand interactions, on the other hand, have a significant impact on docking score and stability. In a preliminary investigation of RMSD, the SARS-CoV-2 spike glycoprotein has been seen at 1.1 Å, and it is constant after the formation of amino acid residues, while the RMSF score is very low at 0.8 Å. For the SARS-CoV-2 alpha variant (PDB ID: 7EKF), the RMSD has been found in Figure 6 in both cases before the development of the amino acid residue and after the formation of the amino acid residue, while it is decreased at RMSF. In Figure 7, the RMSD and RMSF of the SARS-CoV-2 beta variant increased by 0.8 Å before the formation of amino acid residues and shifted to 0.9 Å after the formation of amino acid residues. Similarly, the RMSF score has to decrease slightly more and is approximately 0.7 Å. The RMSD and RMSF of the SARS-CoV-2 gamma variant were 1.1 Å before and 1.2 Å after the development of the amino acid residue, while the RMSF has little impact and decreases by 0.6 Å. The RMSD and RMSF of the SARS-CoV-2 delta variant have been reported to be similar before and after the development of the amino acid residue, which is approximately 0.9 Å and slightly decreases at the point of RMSF (0.7 Å).

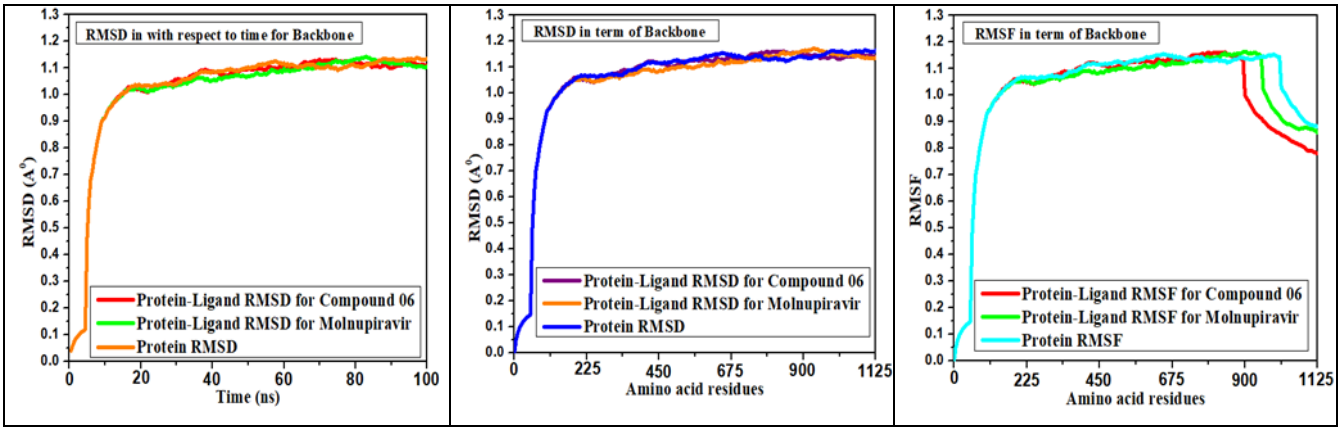

Figure 5. Various RMSD and RMSF SARS-CoV-2 spike glycoproteins (PDB ID: 6vxx)

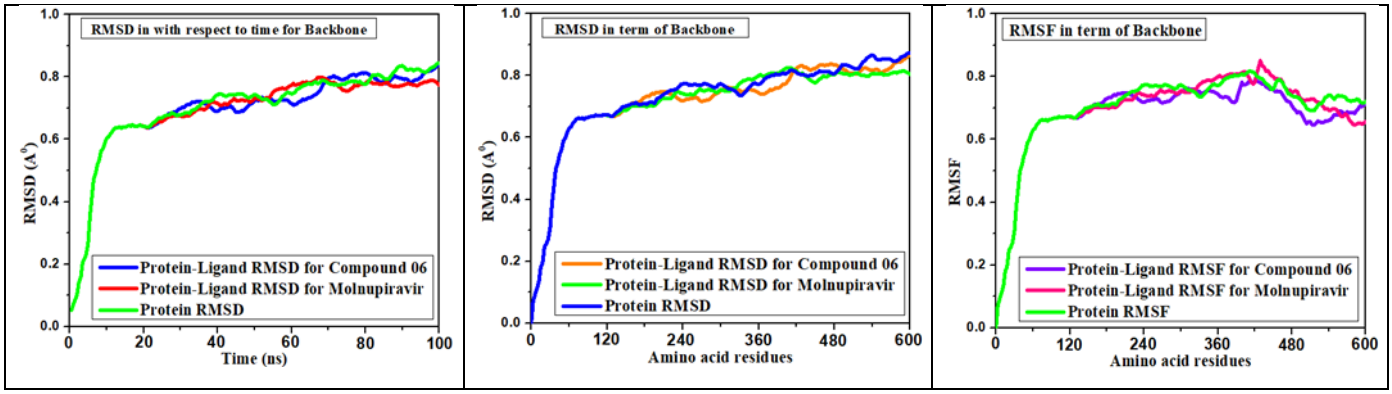

Figure 6. Various RMSD and RMSF SARS-CoV-2 alpha variants (PDB ID: 7EKF)

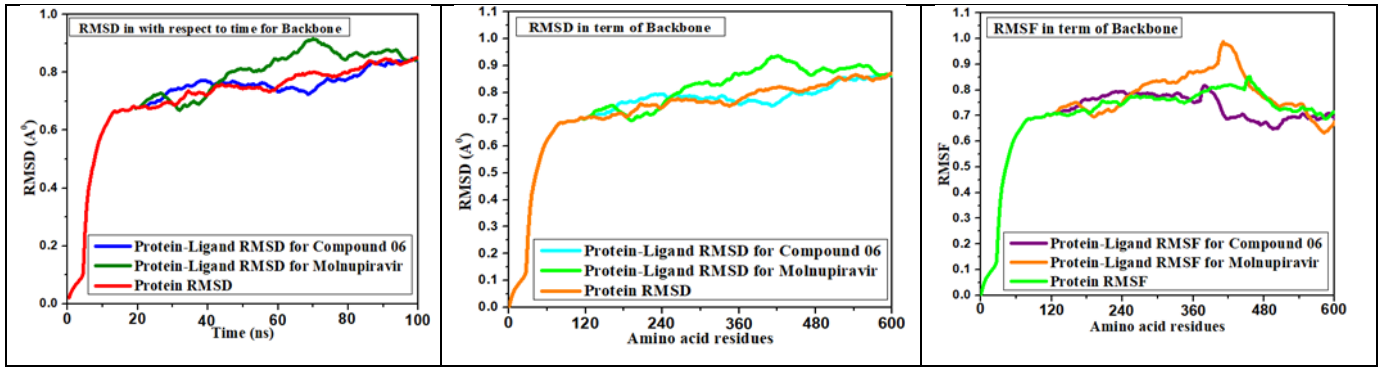

Figure 7. Various RMSD and RMSF values of the SARS-CoV-2 beta variant (PDB ID: 7ekg)

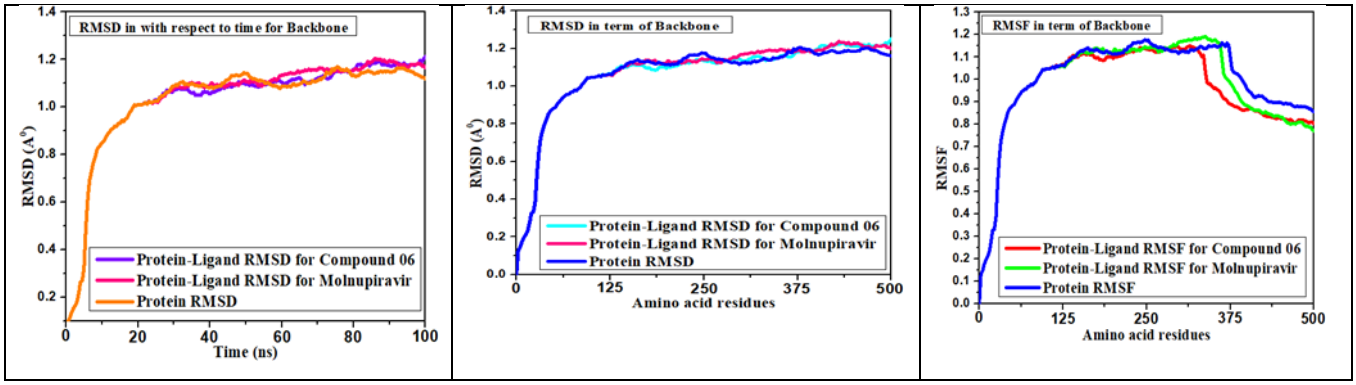

Figure 8. Various RMSD and RMSF values of the SARS-CoV-2 gamma variant (PDB ID: 7V84)

Finally, the RMSD and RMSF of the SARS-CoV-2 Omicron variant were analyzed and are graphically shown in Figure 10. Given this time, the RMSD is 0.8 Å, and the RMSF is 0.6 Å. Therefore, in the conclusion of molecular dynamics simulations, it is clear that the reported

molecule's stability is much better than the standard and may be applied as an alternative and effective treatment against different SARS-CoV-2 variants, such as spike glycoprotein, alpha variant, beta variant, gamma variant, delta variant and omicron variant.

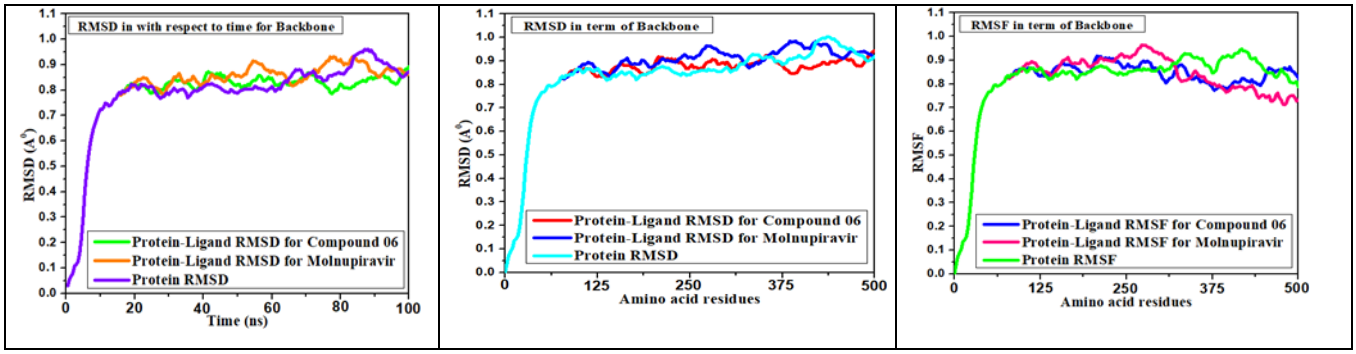

Figure 9. Various RMSD and RMSF values of the SARS-CoV-2 Delta variant (PDB ID: 7V8B)

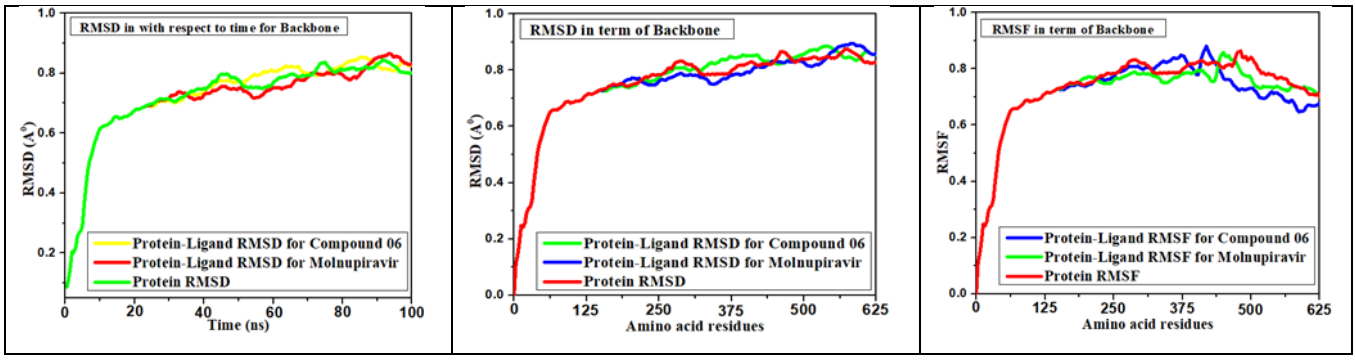

Figure 10. Various RMSD and RMSF values of the SARS-CoV-2 Omicron variant (PDB ID: 7T9J)

3.2 ADMET properties

The results of ADMET calculations, as reported in Table 8, were performed using the pkCSM online server (Pires *et al.*, 2015). ADMET is a designation for absorption, distribution, metabolism, excretion, and toxicity. ADMET capabilities play a crucial role in the initial phases of drug design. Since high-quality drug molecules must have adequate efficacies, potential therapeutic effects and suitable ADMET characteristics at therapeutic dosages. Initially, the standard aqueous solubility range of a drug molecule was considered to be -1 to -5 (Abdul-Hammed *et al.*, 2021). The water solubility range is reported to be between 0.087 and -3.456. Therefore, the Log S values of all of the recommended compounds and standard Log S values are within the range, suggesting that the preferred potent drugs have excellent absorption and distribution capability. Another parameter for the Caco-2 permeability values ranged from approximately -0.136 to 1.05. The volume of distribution is the hypothetical volume across which the complete dosage of medication would have to be evenly distributed to achieve the same amount as that present in blood plasma. Log VDss <-0.15 is considered VDss, whereas Log VDss <0.45 is considered high VDss (Pires *et al.*, 2015). In the prediction, only ligand L01 had Log VDss < -0.227, and the other bioactive molecules had Log VDss predicted to be higher than <0.45. Therefore, it is clear that all the drugs have been highly distributed in plasma, which is an essential pharmacokinetic feature in new drug discovery, and no drugs can reach or distribute through the BBB. The metabolic activities of the suggested pharmacological candidates were also predicted using microsomal enzymes (CYP450 1A2 inhibitor and CYP450 2C9 substrate). All of the listed medications are noninhibitors or nonsubstrates of all cytochrome P450 enzymes, which allows them to be used as possible treatments since they improve their metabolism. The total clearance rate is approximately 0.333 ml/min/kg to 2.189 ml/min/kg,

which indicates that a maximum of 2.189 ml/min/kg of drug excreted from the body and a minimum of 0.333 ml/min/kg could be excreted from the body (Rana *et al*., 2021).

Table 8. ADME properties

Entry	Absorption		Distribution		Metabolism		Excretion	
	Water solubility Log S	Caco-2 Permeability	Log VDss (human)	BBB permeability	CYP450 1A2 Inhibitor	CYP450 2C9 Substrate	Total Clearance (ml/min/kg)	Renal OCT2 substrate
L01	0.087	-0.227	-0.139	No	No	No	0.686	No
L02	-0.413	-0.136	-0.19	No	No	No	0.333	No
L03	-2.908	0.89	-0.689	No	No	No	2.299	No
L04	-2.894	0.781	-1.07	No	No	No	2.089	No
L05	-2.892	0.709	-1.387	No	No	No	2.189	No
L06	-3.456	1.05	-0.511	No	No	Yes	0.436	No
Molnupiravir	-2.852	2.484	0.011	No	Yes	No	-1.493	No

3.2 Aquatic and nonaquatic toxicity

The pharmaceutical industry and regulatory bodies are increasingly relying on in silico approaches to meet the growing demand for quick safety evaluation of pharmaceuticals or medicinal products. These approaches are now being employed worldwide during the development of new drug molecules. All methyl-α-D-mannopyranoside derivatives (L01-L06) are non-AMES-toxic, nonhepatotoxic and nonskin sensitizers when their carcinogenic properties are analyzed, except Molnupiravir, which shows AMES toxicity effects. The oral rat acute toxicity level was measured at 1.457 mol/kg -2.945 mol/kg when the oral rat chronic toxicity level was found to be -1.218 kg_bw/day to 3.729 kg_bw/day (Table 9). Above all, they are regarded as suitable drug candidates.

Table 9. Aquatic and nonaquatic toxicity

Entry	AMES toxicity	Max. tolerated dose (human) mg/kg/day	Oral Rat Acute T Toxicity (LD50) (mol/kg)	Oral Rat Chronic Toxicity (mg/kg_bw/day)	Hepatotoxicity	Skin Sensitization	T. Pyriformis toxicity (Log ug/L)
L01	No	1.858	1.457	3.729	No	No	0.285
L02	No	1.356	1.969	3.252	No	No	0.279
L03	No	0.518	2.45	-1.218	No	No	0.285
L04	No	0.482	2.470	-1.137	No	No	0.285
L05	No	0.457	2.679	-1.451	No	No	0.285
L06	No	0.558	2.945	1.422	No	No	0.285
Molnupiravir	Yes	0.507	2.482	3.976	No	No	0.285

Conclusion

This research work has explained the results of a computational investigation aimed at the discovery and development of new SARS-CoV-2 antagonists against six different variants of SARS-CoV-2. Molecular docking, molecular dynamics, and DFT calculation studies were conducted on D-mannopyranoside derivatives (L01-L06), which could potentially inhibit the SARS-CoV-2 viral pathogen. To make them good and effective therapeutic compounds, pharmacokinetics, ADMET, drug-likeness, HOMO/LUMO, gap, and molecular electrostatic potential and pass prediction investigation studies were also conducted. It has been reported that almost all synthesized bioactive molecules are non-AMES-toxic, nonhepatotoxic and nonskin sensitizers and have much lower HOMO-LUMO energy gaps. When modifying their structure with different aliphatic and aromatic groups, it is conceivable to produce a significant mode of biological activity. The most potent and vital study is molecular docking, which has provided significant docking scores in L06 against SARS-CoV-2 spike glycoprotein, alpha variant, beta variant, gamma variant, delta variant and Omicron variant. All the above docking scores were better than those of the standard Molnupiravir. When docking studies were completed, they were kicked for molecular dynamic simulation, which verified the binding stability of the docked complex. At the end of this research, it is clearly understood that toxicity prediction, in silico ADMET prediction, PASS prediction, and drug-likeness all satisfactorily inhibited and reduced the growth of SARS-CoV-2.

Acknowledgment: The authors are very thankful to the Research & Publication Cell, University of Chittagong [*Ref*: 946/2022-23/2nd Call/04/2023] for providing financial support.

Disclosure statement: *Conflict of Interest:* The authors declare that there are no conflicts of interest.

Compliance with Ethical Standards: This article does not contain any studies involving human or animal subjects.

References

Abdul-Hammed M., Adedotun I.O., Falade V.A., Adepoju A.J., Olasupo S.B., Akinboade M.W. (2021) Target-based drug discovery, ADMET profiling and bioactivity studies of antibiotics as potential inhibitors of SARS-CoV-2 main protease (Mpro), *Virus Dis*., 32(4), 642–656. https://doi.org/10.1007/s13337-021-00717-z

Adrian O.D. (2021) Covid-19: Cases of delta variant rise by 79%, but rate of growth slows, *British Med. J*., 373, 1596. https://doi.org/10.1136/bmj.n1596

Alam A., Rana K.M., Hosen M.A., Dey S., Bezbaruah B., Kawsar S.M.A. (2022) Modified thymidine derivatives as potential inhibitors of SARS-CoV: PASS, *in vitro* antimicrobial, physicochemical and molecular docking studies, *Phys. Chem. Res*., 10(3), 391–409. doi.org/10.22036/pcr.2022.317494.1996

Alam A., Hosen M.A., Hosen A., Fujii Y., Ozeki Y., Kawsar S.M.A. (2021) Synthesis, characterization, and molecular docking against a receptor protein FimH of *Escherichia coli* (4XO8) of thymidine derivatives, *J. Mex. Chem. Soc.*, 65(2), 256–276. https://doi.org/10.29356/jmcs.v65i2.1464

Amin M.R., Yasmin F., Dey S., Mahmud S., Saleh M.A., Emran T.B., Hasan I., Rajia S., Ogawa Y., Fujii Y., Ozeki Y., Kawsar S.M.A. (2021a) Methyl β-D-galactopyranoside esters as potential inhibitors for SARS-CoV-2 Glycoconjugate J protease enzyme: synthesis, antimicrobial, PASS, molecular docking, molecular dynamics simulations and quantum computations, *Glycoconjugate J.*, 39(2), 261–290. https://doi.org/10.1007/s10719-021-10039-3

Amin M.R., Yasmin F., Hosen M.A., Dey S., Mahmud S., Saleh M.A., Hasan I., Fujii Y., Yamada M., Ozeki Y., Kawsar S.M.A. (2021b) Synthesis, antimicrobial, anticancer, PASS, molecular docking, molecular dynamic simulations and pharmacokinetic predictions of some methyl β-D-galactopyranoside analogs, *Molecules*., 26(22), 1–25. https://doi.org/10.3390/molecules26227016

Aanouz I., Belhassan A., El-Khatabi K., Lakhlifi T., El-Ldrissi M., Bouachrine M. (2021) Moroccan medicinal plants as inhibitors against SARS-CoV-2 main protease: Computational investigations, *J. Biomol. Struct. Dyn.*, 39(8), 2971–2979. https://doi.org/10.1080/07391102.2020.1758790

Arifuzzaman M., Islam M.M., Rahman M.M., Mohammad A.R., Kawsar S.M.A. (2018) An efficient approach to the synthesis of thymidine derivatives containing various acyl groups: characterization and antibacterial activities, *Acta Pharm. Sci*., 56(4), 7–22. https://doi.org/10.23893/1307-2080.APS.05622

Becke A.D., (1988) Density-functional exchange-energy approximation with correct asymptotic behavior, *Phys. Rev. A*., 38(6), 3098–3100. https://doi.org/10.1103/physreva.38.3098

Bendaif H., Hammouti B., Stiane I., Bendaif Y., El Ouadi M.A., El Ouadi Y. (2020), Investigation of spread of novel coronavirus (Covid-19) pandemic in Morocco & estimated confinement duration to overcome the danger phase, *Caspian J. Environ. Sci.* 18(1), 13-20

Bulbul M.Z.H., Hosen M.A., Ferdous J., Misbah M.M.H., Chowdhury T.S., Kawsar S.M.A. (2021a) Thermochemical, DFT study, physicochemical, molecular docking and ADMET predictions of some modified uridine derivatives, *Int. J. New. Chem*., 8(1), 88–110. https://doi.org/10.22034/ijnc.2020.131337.1124

Bulbul M.Z.H., Chowdhury T.S., Misbah M.M.H., Ferdous J., Dey S., Hasan I., Fujii Y., Ozeki Y., Kawsar S.M.A. (2021b) Synthesis of new series of pyrimidine nucleoside derivatives bearing the acyl moieties as potential antimicrobial agents, *Pharmacia*., 68(1), 23–34. https://doi.org/10.3897/pharmacia.68.e56543

Case D.A., Cheatham 3rd T.E., Darden T., Gohlke H., Luo R., Merz Jr K.M., Onufriev A., Simmerling C., Wang S., Woods R.J. (2005) The Amber biomolecular simulation programs, *J. Comput. Chem*., 26(16), 1668-1688. https://doi.org/10.1002/jcc.20290

Chtita S., Belaidi S., Qais F.A., Ouassaf M., AlMogren M.M., Al-Zahrani A.A., Bakhouch M., Belhassan A., Zaki H., Bouchrine M., Lakhlifi T., (2022) Unsymmetrical aromatic disulfides as SARS-CoV-2 Mpro inhibitors: Molecular docking, molecular dynamics, and ADME scoring investigations, *J. King Saud Univ. -Sci.*, 34, 102226. https://doi.org/10.1016/j.jksus.2022.102226

Cucinotta D., Vanelli M., (2020) WHO declares COVID-19 a pandemic, *Acta Bio. Medica: Atenei Parmensis*., 91, 157.

Daina A., Michielin O., Zoete V. (2017) SwissADME: a free web tool to evaluate pharmacokinetics, drug-likeness and medicinal chemistry friendliness of small molecules, *Sci. Rep*., 7, 42717. https://doi.org/10.1038/srep42717

Delano W.I., (2002) The PyMOL molecular graphics system, De-Lano Scientific, San Carlos, CA, USA.

Diass K., Oualdi I., Dalli M., Azizi S.-Ed, Mohamed M., Gseyra N., Touzani R., Hammouti B. (2023) Artemisia herba alba Essential Oil: GC/MS analysis, antioxidant activities with molecular docking on S protein of SARS-CoV-2, *Indonesian Journal of Science & Technology* 8(1), 1-18

El Aissouq A., Bouachrine M., Bouayyadi L., Ouammou A., Khalil F. (2023) Structure-based virtual screening of novel natural products as chalcone derivatives against SARS-CoV-2 Mpro, *J. Biomol. Struct. Dyn.*, 1-15. https://doi.org/10.1080/07391102.2023.2172456

El Hadki A., El Hadki H., Tazi R., Komiha N., Zrineh A., El Hajjaji S., Kabbaj O.K. (2021) DFT and molecular docking study of natural molecules proposed for COVID-19 treatment, *Mor. J. Chem.*, 9(2), 198–209. https://doi.org/10.48317/IMIST.PRSM/morjchem-v9i2.21931

Farhana Y., Amin M.R., Hosen M.A., Bulbul M.Z.H., Dey S., Kawsar S.M.A. (2021) Monosaccharide derivatives: Synthesis, antimicrobial, PASS, antiviral, and molecular docking studies against SARS-CoV-2 m^{pro} inhibitors, *J. Cellul. Chem. Technol*., 55(5-6), 477–499. https://doi.org/10.35812/CelluloseChemTechnol.2021.55.44

Fujii Y., Kawsar S.M.A., Matsumoto R., Yasumitsu H., Naoto I., Dohgasaki C., Hosono M., Nitta K., Hamako J., Matsui T., Ozeki Y. (2011) A-D-galactose-binding lectin purified from coronate moon turban, *Turbo (Lunella) coreensis*, with a unique amino acid sequence and the ability to recognize lacto-series glycophingolipids, *Comp. Biochem. Physiol*., 158B(1), 30–37. doi.org/10.1016/j.cbpb.2010.09.002

Guan L., Hongbin Y., Yingchun C., Lixia S., Peiwen D., Weihua L., Guixia L., Yun T. (2019) ADMET-score–a comprehensive scoring function for evaluation of chemical drug-likeness, *Medchemcomm*., 10(1), 148–157. https://doi.org/10.1039/c8md00472b

Hosen M.A., Munia N.S., Al-Ghorbani M., Baashen M., Almalki F.A., Hadda T.B., Ali F., Mahmud S., Saleh M.A., Laaroussi H., Kawsar S.M.A. (2022) Synthesis, antimicrobial, molecular docking and molecular dynamics studies of lauroyl thymidine analogs against SARS-CoV-2: POM study and identification of the pharmacophore sites, *Bioorg Chem.*, 125, 105850. https://doi.org/10.1016/j.bioorg.2022.105850

Huang X., Wei F., Hu L., Wen L., Chen K., (2020) Epidemiology and clinical characteristics of COVID-19, *Arch. Iran. Med*., 23, 268–271.

Islam S., Hosen M.A., Ahmad S., ul Qamar M.T., Dey S., Hasan I., Fujii Y., Ozeki Y., Kawsar S.M.A. (2022) Synthesis, antimicrobial, anticancer activities, PASS prediction, molecular docking, molecular dynamics and pharmacokinetic studies of designed methyl α-D-glucopyranoside esters, *J. Mol. Struct*., 1260, 132761. https://doi.org/10.1016/j.molstruc.2022.132761

Kabir A.K.M.S., Kawsar S.M.A., Bhuiyan M.M.R., Islam M.R., Rahman M.S. (2004) Biological evaluation of some mannopyranoside derivatives, *Bull. Pure Appl. Sci*., 23(2), 83-91.

Kabir A.K.M.S., Kawsar S.M.A., Bhuiyan M.M.R., Rahman M.S., Banu B. (2008) Biological evaluation of some octanoyl derivatives of methyl 4,6-O-cyclohexylidene-α-D-glucopyranoside, *Chittagong Univ. J. Biol. Sci*., 3(1&2), 53-64.

Kabir A.K.M.S., Kawsar S.M.A., Bhuiyan M.M.R., Rahman M.S., Chowdhury M.E. (2009a) Antimicrobial screening of some derivatives of methyl α-D-glucopyranoside, *Pak. J. Sci. Ind. Res.*, 52(3), 138-142.

Karim S.S.A., Karim Q.A., (2021) Omicron SARS-CoV-2 variant: a new chapter in the COVID-19 pandemic, *Lancet*., 398(10317), 2126–2128. https://doi.org/10.1016/S0140-6736(21)02758-6

Kawsar S.M.A., Ferdous J., Mostafa G., Manchur M.A. (2014) A synthetic approach of D-glucose derivatives: spectral characterization and antimicrobial studies, *Chem. Chem. Technol*., 8(1), 19–27. https://doi.org/10.23939/chcht08.01.019

Kawsar S.M.A., Mostafa G., Huq E., Nahar N., Ozeki Y. (2009) Chemical constituents and hemolytic activity of *Macrotyloma uniflorum* L., *Int. J. Biol. Chem.*, 3(1), 42-48.

Kawsar S.M.A., Hamida A.A., Uddin S.A., Hossain M.K., Chowdhury S.A., Sanaullah A.F.M., Manchur M.A., Hasan I., Ogawa Y., Fujii Y., Koide Y., Ozeki Y. (2015) Chemically modified uridine molecules incorporating acyl residues to enhance antibacterial and cytotoxic activities, *Int. J. Org. Chem*., 5(4), 232-245. https://doi.org/10.4236/ijoc.2015.54023

Kawsar S.M.A., Hosen M.A., Fujii Y., Ozeki Y. (2020a) Thermochemical, DFT, molecular docking and pharmacokinetic studies of methyl β-D-galactopyranoside esters, *J. Comput. Chem. Mol. Model*., 4(4), 452–462. https://dx.doi.org/10.25177/JCCMM.4.4.RA.10663

Kawsar S.M.A., Hosen M.A. (2020b) An optimization and pharmacokinetic studies of some thymidine derivatives, *Turk. Comput. Theor. Chem*., 4(2), 59–66. https://doi.org/10.33435/tcandtc.718807

Kawsar S.M.A., Kumar A. (2021a) Computational investigation of methyl α-D-glucopyranoside derivatives as inhibitor against bacteria, fungi and COVID-19 (SARS-2), *J. Chil. Chem. Soci*., 66(2), 5206–5214. https://www.jcchems.com/index.php/JCCHEMS/article/view/1757

Kawsar S.M.A., Hosen M.A., Alam A., Islam M., Ferdous J., Fujii Y., Ozeki Y. (2021b) Thymidine derivatives as inhibitors against novel Coronavirus (SARS-CoV-2) main protease: theoretical and computational investigations, *Adv. Chem. Res*., 69,89–129.

Kawsar S.M.A., Kumar A., Nasrin S.M., Hosen M.A., Chakma U., Akash S. (2022) Chemical descriptors, PASS, molecular docking, molecular dynamics and ADMET predictions of glucopyranoside derivatives as inhibitors to bacteria and fungi growth, *Org. Commun*., 15(2), 184–203. http://doi.org/10.25135/acg.oc.122.2203.2397

Kawsar S.M.A., Ryo M., Fujii Y., Matsuoka H., Masuda N., Chihiro I., Yasumitsu H., Kanaly R.A., Sugawara S., Hosono M., Nitta K., Ishizaki N., Dogasaki C., Hamako J., Matsui T., Ozeki Y. (2011)

Cytotoxicity and glycan-binding profile of α-D-galactose-binding lectin from the eggs of a Japanese sea hare (*Aplysia kurodai*), *The Protein J.* 30(7), 509–519. https://doi.org/10.1007/s10930-011-9356-7

Kawsar S.M.A., Hosen M.A., Chowdhury T.S., Rana K.M., Fujii Y., Ozeki Y. (2021c) Thermochemical, PASS, molecular docking, drug-likeness and in silico ADMET prediction of cytidine derivatives against HIV-1 reverse transcriptase, *Rev. de Chim.*, 72(3), 159-178. https://doi.org/10.37358/RC.21.3.8446

Khatabi K.E., Aanouz I., Alaqarbeh M., Ajana M.A., Lakhlifi T., Bouachrine M. (2022) Molecular docking, molecular dynamics simulation, and ADMET analysis of levamisole derivatives against the SARS-CoV-2 main protease (MPro), *BioImpacts* 12(2), 107–113. https://doi.org/10.34172/bi.2021.22143

Kumer A., Chakma U., Islam M.T., Howlader D., Hossain T. (2021) The computational investigation of sixteen antiviral drugs against main protease (mpro) and spike protease (spro) of sars-COV-2, *J. Chil. Chem. Soc*., 66, 5339–5351.

Li M., Lou F., Fan H. (2021) SARS-CoV-2 Variants of Concern Delta: a great challenge to prevention and control of COVID-19, *Signal Transduct. Target Ther*., 6, 1–3. https://doi.org/10.1038/s41392-021-00767-1

Lipinski C.A., Lombardo F., Dominy B.W., Feeney P.J. (2001) Experimental and computational approaches to estimate solubility and permeability in drug discovery and development, *Adv. Drug Deliv. Rev.*, 46, 3–26.

Mandal N., Padhi A.K., Rath S.L. (2022) Molecular insights into the differential dynamics of SARS-CoV-2 variants of concern, *J. Mol. Graph Model*., 114, 108194. https://doi.org/10.1016/j.jmgm.2022.108194

Maowa J., Hosen M.A., Alam A., Rana K.M., Fujii Y., Ozeki, Y., Kawsar S.M.A., (2021a) Pharmacokinetics and molecular docking studies of uridine derivatives as SARS- COV-2 M^{pro} inhibitors, *Phys. Chem. Res*., 9(3), 385–412. https://doi.org/10.22036/pcr.2021.264541.1869

Maowa J., Alam A., Rana K.M., Hosen A., Dey S., Hasan I., Fujii Y., Ozeki Y., Kawsar S.M.A. (2021b) Synthesis, characterization, synergistic antimicrobial properties and molecular docking of sugar modified uridine derivatives, *Ovidius Univ. Ann. Chem*., 32(1), 6–21. doi.org/10.2478/auoc-2021-0002

Mirajul M.I., Arifuzzaman M., Monjur M.R., Rahman A., Kawsar S.M.A. (2019) Novel methyl 4,6-*O*-benzylidene-α-D-glucopyranoside derivatives: synthesis, structural characterization and evaluation of antibacterial activities, *Hacettepe J. Biol. Chem*., 47(2), 153–164. doi.org/10.15671/hjbc.622038

Misbah M.M.H., Ferdous J., Bulbul M.Z.H., Chowdhury T.S., Dey S., Hasan I., Kawsar S.M.A. (2020) Evaluation of MIC, MBC, MFC and anticancer activities of acylated methyl β-D-galactopyranoside esters, *Int. J. Biosci*., 16(4), 299-309. http://dx.doi.org/10.12692/ijb/16.4.299-309

Nath A., Kumer A., Zaben F., Khan W.M. (2021) Investigating the binding affinity, molecular dynamics, and ADMET properties of ihydrobenzofuran derivatives as an inhibitor of fungi, bacteria, and virus protein, *Beni-Suef Univ. J. Basic Appl. Sci*., 10, 1-13. https://doi.org/10.1186/s43088-021-00117-8

Paraskevis D., Kostaki E.G., Magiorkinis G., Panayiotakopoulos G., Sourvinos G., Tsiodras S. (2020) Full-genome evolutionary analysis of the novel corona virus (2019-nCoV) rejects the hypothesis of emergence as a result of a recent recombination event, *Infect. Genet. Evol*., 79, 104212. https://doi.org/10.1016/j.meegid.2020.104212

Parr R.G. (1980) Density functional theory of atoms and molecules in Horizons of quantum chemistry, *Springer*, 5-15.

Phillips J.C., Braun R., Wang W., Gumbart J., Tajkhorshid E., Villa E., Chipot C., Skeel R.D., Kalé L., Schulten K. (2005) Scalable molecular dynamics with NAMD, *J. Comput. Chem*., 26(16), 1781–1802. https://doi.org/10.1002/jcc.20289

Pires D.E.V., Blundell T.L., Ascher D.B. (2015) pkCSM: predicting small-molecule pharmacokinetic and toxicity properties using graph-based signatures, *J. Med. Chem*., 58(9), 4066–4072. https://doi.org/10.1021/acs.jmedchem.5b00104

Rana K.M., Maowa J., Alam A., Dey S., Hosen A., Hasan I., Fujii Y., Ozeki Y., Kawsar S.M.A. (2021) In silico DFT study, molecular docking, and ADMET predictions of cytidine analogs with antimicrobial and anticancer properties, In Silico *Pharmacol*., 9(1), 42. https://doi.org/10.1007/s40203-021-00102-0

Saputra H., Albar C. N., Soegoto D. S. (2022) Bibliometric analysis of computational chemistry research and its correlation with Covid-19 Pandemic, *Mor. J. Chem.* 10(1), 37-49, https://doi.org/10.48317/IMIST.PRSM/morjchem-v10i1.31723

Shagir A.C., Bhuiyan M.M.R., Ozeki Y., Kawsar S.M.A. (2016) Simple and rapid synthesis of some nucleoside derivatives: structural and spectral characterization, *Curr. Chem. Lett*., 5(2), 83–92. https://doi.org/10.5267/j.ccl.2015.12.001

Shamsuddin T., Hosen M.A., Alam M.S., Emran T.B., Kawsar S.M.A., (2021) Uridine derivatives: antifungal, PASS outcomes, ADME/T, drug-likeliness, molecular docking and binding energy calculations, *Med. Sci. Int. Med. J*., 10(4), 1373–1386. https://doi.org/10.5455/medscience.2021.05.175

Shuxian Z., Zezhou W., Ruijie C., Huwen W., Chen X., Xiaoyue Y., Lhakpa T., Yinqiao D., Hui W., Yong C. (2020) COVID-19 containment: China provides important lessons for global response, *Front. Med*., 14, 215–219. https://doi.org/10.1007/s11684-020-0766-9

Soudani W., Zaki H., Alaqarbeh M., ELMchichi L., Bouachrine M., Hadjadj-Aoul F.Z. (2023) Discover the medication potential of Algerian medicinal plants against SARS-CoV-2 main protease (Mpro): Molecular docking, molecular dynamic simulation, and ADMET analysis, *Chem. Afr.*, 1–17. https://doi.org/10.1007/s42250-023-00684-6

Tang A., Zhen-Dong T., Hong-Ling W., Ya-Xin D., Ke-Feng L., Jie-Nan L., Wen-Jie W., Chen Y., Meng-Lu Y., Peng L., Jian-Bo Y. (2020) Detection of novel coronavirus by RT–PCR in stool specimen from asymptomatic child China, *Emerg. Infect. Dis*., 26, 1337–1339.

Touzani R., Hammouti B., Almalki F.A., Ben Hadda T. (2020) Coronavirus, Covid19, Covid-19 and SARS-Cov-2: A Global Pandemic, A Short Review, *J. Mater. Environ. Sci.*, 11(4), 736-750

Version A.D.S., 4.0., Accelrys, San Diego, USA, 2017.

Weymouth-Wilson A.C. (1997) The role of carbohydrates in biologically active natural products, *Nat. Prod*., 14(2), 99–110. . https://doi.org/10.1039/np9971400099

Xia S., Zuoling W., Lijue W., Qiaoshuai L., Fanke J., Linhua T., Qian W., Fei S., Shibo J. (2021) Structure-based evidence for the enhanced transmissibility of the dominant SARS-CoV-2 B. 1.1. 7 variant (Alpha), *Cell Discov*., 7(1), 1–5. https://doi.org/10.1038/s41421-021-00349-z

Zhang D., Min H., Qiang J., (2020) Financial markets under the global pandemic of COVID-19, *Finance Res. Lett*., 36, 101528. https://doi.org/10.1016/j.frl.2020.101528

Zucman N., Fabrice U., Descamps D., Roux D.R., Jean-Damien R. (2021) Severe reinfection with South African SARS-CoV-2 variant 501Y. V2: A case report, *Clin. Infect. Dis*., 73(10), 1945–1946. https://doi.org/10.1093/cid/ciab129